

Investigation of Short Pulse Nd:YAG Laser Interaction with Stainless Steel Powder Beds

W. O'Neill, C.J. Sutcliffe, R. Morgan & K.K.B. Hon

Department of Engineering
Manufacturing Engineering & Industrial Management
University of Liverpool
United Kingdom

Abstract

The development of metallic object construction has occurred at quite a pace over the last five years with provision of many commercial techniques such as indirect and direct sintering of metal powder beds. Although porosity is still a major problem for metal building a number of notable solutions have been proposed, these include infiltration with low melting point alloys or direct fusing with binary powder mixtures. Neither of these solutions allows one to build components without compromising part strength and functionality. A process route is required that will allow solid parts to be built from a single powder component without requiring time consuming downstream processes. To this end, the present work examines the feasibility of using low energy high peak power laser pulses from a Q-switched Nd:YAG laser to melt stainless steel powder fractions whilst examining the melt displacement through high recoil pressures induced by rapid partial vaporisation of the powder layer. The effect of laser pulse energy, laser beam intensity, pulse frequency, and environmental gas control on the integrity of the fused powder layer is presented.

1.0 Introduction

The introduction of Rapid Production Technologies (RPT) into modern manufacturing has been received with great applause from product designers and manufacturing engineers. The use of RPT has facilitated shorter lead times on product development and the ability to produce design iterations without the time and cost penalties associated with traditional product development cycles. Rapid prototyping quickly emerged as a completely new tool for product development tasks which in turn initiated a number of research and development programmes for rapid tooling processes that allowed small batch production to become cost effective. The manufacturing engineer has a wealth of small to medium batch processes such as investment casting, vacuum casting, AIMSTM tooling, KeltoolTM and RapidtoolTM. Whilst these processes provide sufficient scope for injection mould tooling certain compromises have to be made with regard to lifetime, lead-time, material properties, accuracy and scale. These compromises must be eradicated if we are to realise true rapid manufacturing for both functional components and tooling.

Of the main RPT processes selective laser sintering provides the widest range of build materials which include a variety of polymers and a number of metal based materials. The accuracy of parts produced by SLS is no greater than that achieved with stereolithography, although the ability to produce functional parts directly from the SLS build chamber gives the SLS process considerable advantages over other RPT. When it comes to metallic object construction there are a number of SLS methods which have been used as shown in Figure 1.

Direct metal sintering relies on laser induced melting to couple powder particles together, significant thermal gradients exist using this route unless the powder bed temperatures are controlled to a value just short of the powder melt temperature. This approach reduces problematic temperature gradients and produces parts with minimum internal stresses. Porosity is still a problem which is normally reduced by post sintering or infiltration.

Indirect sintering of metals relies on melting of the polymer coating on each metal particle, this "green" part can then be handled with subsequent de-binding, sintering and low melting point infiltration stages which are necessary to produce a solid high density part [1,2].

Binary phase sintering has been investigated by a number of workers [3,4,5]. This process involves the illumination of a composite powder mixture such that a particular phase of the powder is melted in preference to the other. Examples of binary mixtures include Cu-Ni; Fe-Co; W-Mo. The low melting point components are employed to effect bonding within the mixture.

Objects built via the above routes are generally not suited for heavy duty functional parts since the majority of infiltrates and binary phase materials are low melting point metals with low mechanical strength. Parts produced thus have the strength and performance characteristics of their weakest composite phase. The production of fully functional parts requires processing routes that result in near 100% density from a single powder, i.e., stainless steel, tool steels, titanium etc. It is clear from the literature that there have been few attempts to condition the laser-material interaction such that laser induced non-thermal effects are generated to aid the melting and densification of powder beds in a single step. To this end, this work presents preliminary results of laser induced high pressure direct sintering of 316 stainless steel powder beds.

2.0 Background

The majority of laser based RPT utilise CO₂ gas lasers or in some cases solid-state Nd:YAG lasers. In commercial applications of SLS a 50W or 100 W CO₂ laser are used to thermally activate the powder bed. If melting occurs the process relies on surface tension driven melt displacement to distribute the molten volume and bond nearest particles into a conglomerate that is near full density or significantly less than full density, depending upon the interaction parameters. Fusion based processes of this kind are very susceptible to unwanted thermal gradients which reduce the chance of wetting leading to balling phenomena and poor layer properties. It is useful at this stage to examine the traditional approach to making components from metal powder. Conventional powder metallurgy processes use high temperatures and high pressures to squeeze powder beds into shapes formed by mould cavities or dies [6]. The high pressures ensure high levels of compaction and even at room temperature one can approach the full density of the material when multi-modal powders are used. The application of heat provides the energy necessary for transfer of matter from one particle to the other resulting in a strong diffusion based solid-state bond allowing full densities to be achieved. None of these processes occur in conventional selective laser sintering of metals, the pressures are too low by several orders of magnitude, the laser interaction duration is too short by several hundred orders of magnitude. Table.1 gives typical pressures and temperatures used in the powder metallurgy industry for part forming and sintering.

One can see from Table.1 that SLS processes operating at atmospheric pressure are severely handicapped in terms of high density part production. It is for this reason that downstream infiltration and sintering processes are used in conjunction with SLS to increase part functionality and strength.

Attainment of the temperatures presented in Table 1 are not difficult with laser powers even as low as 50W. The SLS systems are capable of melting most materials even ceramics, indeed their ability to fuse materials is the basis of all SLS processes. Interaction times to promote diffusion of matter between particles and promote necking are typically several minutes or longer. Given that the laser

illuminates small areas for definition of part geometry, the dwell time per unit area is generally of the order of milliseconds, much too short to promote solid-state bonding.

It is well known that surface tension forces play an important role in shaping the melt beads that are generated in direct SLS of metals. Cold powder beds will often lead to minimal wetting between the powder bed and the melt bead. Increasing the bed temperature to several hundred degrees Celsius will increase wetting and melt bead balling reduces thereby allowing greater control over part geometry. Unfortunately, there is the possibility that other natural forces are at work which lead to modifications of the melt bead shape, namely Marangoni forces. Marangoni forces are the result of steep temperature gradients across the melt bead that generate surface tension gradients which in turn generate convective mass transfer and local reciprocal stirring of the melt volume. This effect is recognised in laser welding and has a significant effect on the melt geometry. It is likely that under continuous wave laser illumination Marangoni flow may be occurring in the melt bead generated on the surface of the powder bed, although it is not known to what extent it influences the melt bead geometry in this case.

In pulsed laser interactions there is the strong possibility of plasma generation which in turn will lead to forces that allow for modification of the melt pool and hence the shape of the laser generated bead. This is a particularly interesting avenue since it may lead to more controllable bead formation which in turn may increase part accuracy and particularly part density. Consider the situation shown in Figure 2, a pulsed laser interacts with a leveled powder bed over nanosecond time scales such that the peak pulse powers are of the order of several hundred kilo Watts for average powers of around 100W. Rapid heating of the substrate occurs which produces melting, vaporisation and finally partial ionisation of the vapour. The partial ionisation or plasma is fed by vaporised matter leaving the surface of the substrate at velocities up to 10^5 m/s. The net result is a shock wave travelling toward the laser beam and a recoil shock travelling away from the laser beam and into the substrate. Recoil pressures of the order of 400 MPa are possible with peak power densities of the order of several GWcm^{-2} [7]. This regime is of interest to the authors as it may provide the pressures necessary for localised melt/powder compaction which will produce higher density parts than is possible with continuous wave (CW) laser beams. It is also possible that a second benefit may be the ability of the recoil shocks to overcome surface tension forces and prevent balling of the melt pool (enforced wetting).

It is clear that a balance must be sought between melt production and shock formation, excessive pressures will lead to explosive removal of the powder bed rather than melt displacement. This paper presents the results of a preliminary examination of the interaction characteristics of nanosecond laser pulses and stainless steel powder beds.

3.0 Experimental Arrangement

An experimental SLS test facility was constructed consisting of a Rofin Sinar 90W flash-lamp pumped Q-switched Nd:YAG laser with a frequency range of 0 to 60 kHz. Typical pulse energies and pulse widths were in the range 0.2-3 mJ and 80-250 ns respectively. The laser was apertured in order improve the mode quality and therefore focusability of the beam. Plots of laser power output verses pulsing frequency are shown in Figure 3 for a number of lamp currents in the range 12-20 Amps. One can see that continuous wave operation (CW) provides the highest average output power of 15W at 20 Amps lamp current. Powers quoted here are measured at the surface of the powder bed. Line scanning was achieved using a RSG1014 galvanometer scanning head containing 2 thermally regulated S10 galvanometers giving a scanning speed range of 1-500 mm/s over an 80mm by 80mm area. The focal length of the imaging lens was 112mm giving a minimum spot size of 50 μm .

Computer control of both laser parameters and scanning is accomplished using an IBM compatible PC running Rofin Sinar's LaserWorkbench software under the OS2 operating system. This software not only allows scanning of many image types but also enables programming of scanning trajectory and the setting of all process variables from within a Pascal based programming language.

The build chamber consists of a build cylinder and powder delivery cylinder each 100 mm diameter powered by 2 linear stepping motors with minimum step size of 0.25 microns and maximum stepping rate of 380 steps per second. 316L Stainless powder with a mode size of 20 μ m is delivered to the build chamber by a 70 mm diameter counter rotating roller driven by a DC servo motor. The build chamber is computer controlled via a PC based SM30 3-axis stepper motor controller which simultaneously controls powder feeder, build platform and sweeper assembly. In house control software was used to link the laser system with the SLS build chamber thereby effecting full control over the experimental system. This preliminary investigation made no attempt to control powder bed temperatures in order to identify the benefits of the plasma initiated high pressure interaction.

4.0 Experimental Procedures

Powder beds some 300 μ m thick were metered onto the build platform. After a suitable purging operation the chamber was filled with Ar shroud gas (99.999%) in order to minimise oxidation effects. This is particularly important with Stainless Steel powders as the melt temperature of the chromium oxide is substantially higher than that of iron which causes problems when super heated pockets of molten iron are trapped within a "bag" of chromium oxide. Further heating of these oxide "bags" leads to catastrophic failure and explosive release of molten iron which dramatically reduces the controllability of the process.

A series of interaction trials were run to characterise the general nature of the interaction for a number of parameters and classify the interaction site in terms of the observed effects as a function of the value of the parametric variables i.e. crater formation, balling and melting. The parametric variables were: frequency f 0-60kHz; scanning velocity v 100mms⁻¹; Lamp current I 0-20Amps; peak power density P_p 2kW-1.4GWcm⁻², Scan line overlap 25% of line width. The system configuration enabled a matrix of 100 parametric values to be tested at once which made data collection highly efficient and allowed easy comparisons to be made between the data sets. A schematic example of the arrangement is shown in Figure 4. Sintered pads of around 3mmx3mm were produced for a selection of data within the parametric variable range.

5.0 Results and Discussion

Figure 5 is a photograph of the undisturbed powder bed at 50x magnification with an insert photograph at 500x magnification. One can see that in general the mode of the powder is lower than the 20 μ m as given by the manufacturer. Low mode numbers are preferred in this work due to the small laser beam diameters that can be achieved with the experimental arrangement. Although low mode numbers make powder handling more difficult they generally increase laser beam absorption compared to high mode numbers. A full set of single layer interactions were investigated for a range of parameters. Within the grid array described above it is possible to change pulse frequency and laser power and produce a single layer pad for each pair of parameters. The results of these investigations produce a process map which have been analysed by optical and scanning electron microscopy. The following sections discuss the general features of the process maps for three laser spot diameters, 50 μ m, 150 μ m and 300 μ m. We have chosen to view the results obtained at varying spot diameter rather than speed because changes in spot diameter will significantly affect recoil pressures induced on the target powder bed.

5.1 Laser Spot Diameter: 50 μ m

Using a laser spot diameter of 50 μ m allows significant recoil pressures to be generated on the powder bed. These are so great that significant levels of powder are blasted from the interaction site preventing samples from fusing. Figure 6 gives the process map for this spot diameter. One can see that a threshold current of 1.9 A is required in order to initiate melting, this is the case throughout the frequency range of 0-60kHz. In the case of the continuous laser beam (CW) pads were produced which could be handled at a current level of 11.9A. Pads produced above this limit suffered an increased surface roughness with current. A distinct region of high recoil pressures is realised above 6.6 kHz with the region extending to high frequencies as the lamp current is increased. Low frequencies give high peak powers per pulse and result in large shock formations accompanied by bright plasma plumes characteristic of an ion plasma. In this region the powder bed was blasted away. Increasing the pulse frequency reduces peak powers and although shock waves are present they are incapable of displacing significant amounts of powder. In this region the pads were melted and could be handled quite easily. Operating above 40kHz and 18.8 Amps produced pads that were fused to the holding platform which was some 300 μ m below the top of the powder layer.

5.2 Laser Spot Diameter: 150 μ m

Increasing the spot diameter allows one to change both the given peak power density and the area of the interaction per pulse. In this section the results for a spot diameter of 150 μ m are presented which represents a substantial decrease in peak power density compared to that at 50 μ m. This subsequent reduction in peak power density has reduced the scale of powder displacement although lamp currents above 12.5 A and frequencies up to 40kHz produce volumes of powder displacement which prevent the formation of single layer pads. The zone of effective fusion is shown on the top right of Figure 7. Surface roughness scales with lamp current as melt volumes increase and surface tension forces induce slight balling phenomenon.

5.3 Laser Spot Diameter: 300 μ m

In this section the data for a spot diameter of 300 μ m is presented. As can be seen from Figure 8 the peak powers have reduced to the point that powder remains in contact with the bed and damaging recoil pressures are absent throughout the range of parameters. The usual threshold for significant particle melting is present at around 12.0 Amps. Increasing the lamp current for a particular pulse frequency serves to raise melt volumes and surface tension forces pull the pads into a rough featured layer. In this data set the effects of curl are beginning to show which is indicative of thermal stresses induced by the temperature gradients within the powder bed. It is interesting to note that the smaller spot diameters produced little evidence of curling.

5.4 Scanning Electron Micrographs

In order to identify specific features in the fused zones it is necessary to use scanning electron microscopy. The density of the layers is important in that the objective of the research is to produce a solid metal build process without the need for downstream processing routes such as infiltration or upstream processing routes such as binary phase mixtures. In this respect the samples were analysed for variations in the observed porosity under high magnification. The results are presented below.

Figure 9 presents photomicrographs at a magnification of 50x for three pads produced with a beam diameter of 150 μ m and the following beam parameters: 9a) CW @ 20A, 15W; 9b) 40kHz @ 20A, 11W average; 9c) 60kHz @ 20A, 12.6W average. Refer to figure.7 for their position on the process map at 150 μ m diameter. One can see that the CW sample is exhibiting fusion along the scanning direction (left to right), with high levels of porosity between scans. Figure 9b shows less balling with little evidence of a visible line scan direction. Surface melt would have little time to flow in the pulsed interaction due to the extremely short freeze-out times associated with heating *and* cooling on nanosecond time-scales. Although blast waves from rapid surface heating could conceivably displace the melt during its lifetime. Figure 9c shows the pad surface at a frequency of 60kHz. In this case we have a surface which is less porous than 9a or 9b.

Figure 10 presents photomicrographs at a magnification of 50x for three pads produced with a beam diameter of 300 μ m and the following beam parameters: 10a) CW @ 20A, 15W; 10b) 20kHz @ 20A, 10W average; 10c) 40kHz @ 20A, 11W average; 10d) 60kHz @ 20A, 12.6W average; Refer to figure.8 for their position on the process map. Figure 10a, the CW sample, shows significant fusion and melt flow with high levels of porosity at the surface still evident. The scan lines in this case are at 45 degrees to the horizontal and can be seen to be the planes of maximum porosity. Figure 10b gives the surface of a pad produced at two thirds the power of sample 10a and is exhibiting less porosity and no evidence of scanning direction. This trend increases with pulse frequency until the maximum at 60 kHz. Here, Figure 10d, shows almost zero surface porosity and has no evidence of the scanning direction.

There is clearly a difference between the interaction of a pulsed laser beam and one operating continuously. We have argued that recoil pressures associated high peak powers may improve the density of laser fused metal powder beds to some degree. The above results, especially those of Figure 10, indicate that melt movement is affected by the pulsed interaction. It is not clear what the mechanism is at this stage of the investigation. All of the above samples have been produced at high lamp currents. The effect of pulsed illumination is shown more clearly in Figure 11 with samples produced at a lamp current of 13.3 Amps at 60 kHz and CW operating modes. It is clear that in Figure 11a that continuous illumination has aided melt displacement through surface tension forces, unlike that of Figure 11b where the melt has been fused in-situ with almost no movement. Greater understanding of this phenomenon requires more data. To this end experiments are in progress to examine the pulsed illumination event in greater detail.

6.0 Conclusions

This work has presented preliminary results of the interaction effects of short pulsed Nd:YAG laser light on 316 Stainless Steel powder beds. Results have indicated that improvement in surface quality can be achieved with optimised laser beam interaction parameters. The mechanisms that are at work in the case of pulsed illumination are not fully understood. Further experiments are in hand to gain more information on the means by which pulsed laser light affects the surface of powder beds.

7.0 Acknowledgements

The authors would like to thank the EPSRC and Lever Brothers PLC for their support of this program through a ROPA grant, in particular we are indebted to Mr Jim Rait of Lever Brothers PLC for his financial support and encouragement during the course of this work. We would also like to thank Mr. Lawrence Bailey, a technician on the project for his invaluable assistance during the design and fabrication stages of the build chamber.

8.0 References

1. Badrinarayan, B. "study of the selective laser sintering of metal-polymer powders", PhD thesis, University of Texas at Austin, Austin, Texas, 1995.
2. Badrinarayan, B., Barlow, J.W., "Prediction of the thermal conductivity of beds which contain polymer coated metal particles", Proc. Solid Freeform Fabrication, University of Texas at Austin, Austin, Texas, pp91-97, 1990.
3. Manriquez-Frayre, J.A., & D.L. Bourell, "Selective laser sintering of binary metallic powder", Proc. Solid Freeform Fabrication, University of Texas at Austin, Austin, Texas, pp99-106, 1990.
4. Manriquez-Frayre, J.A., & D.L. Bourell, "Selective laser sintering of Cu-Pb/Sn solder powders", Proc. Solid Freeform Fabrication, University of Texas at Austin, Austin, Texas, pp252-260, 1991.
5. Nyrhila, O, "Manufacture of dimensionally precise pieces by sintering", US Patent, 5061-439, 1991.
6. Kuhn, H.A., and Ferguson, B.L., "Powder Forging", Princeton, N.J., Metal Powder Industries Federation, 1990.
7. Kyo-Dong, S. and Alexander, D.R., "Propagation velocities of laser produced plasmas from copper wire targets and water droplets", J.App.Phys, 76 (6), 3302-3312, (1994).

Table.1 Typical operating parameters for traditional sintering processes

Material	Pressure (MPa)	Temperature (°C)	Duration (Min)
Stainless Steels	370-875	1100-1290	30-60
Brass	400-700	760-900	10-45
Bronze	200-275	1100-1290	30-60
Iron	350-800	1000-1150	8-45
Cemented Carbides	140-400	1430-1500	20-30

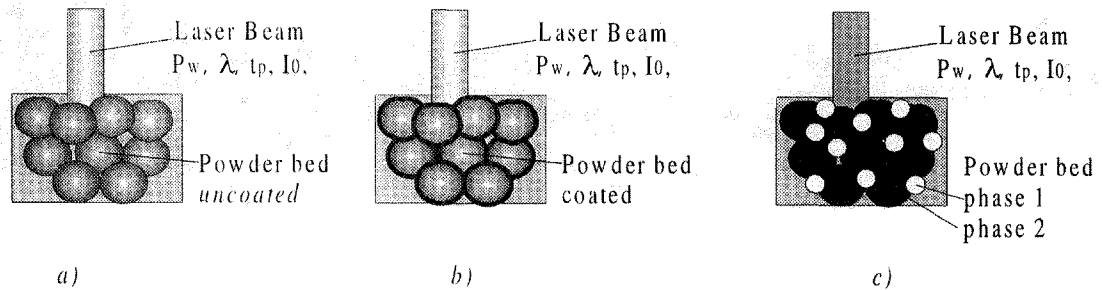


Figure.1 a) direct metal sintering, b) indirect sintering, c) binary phase sintering

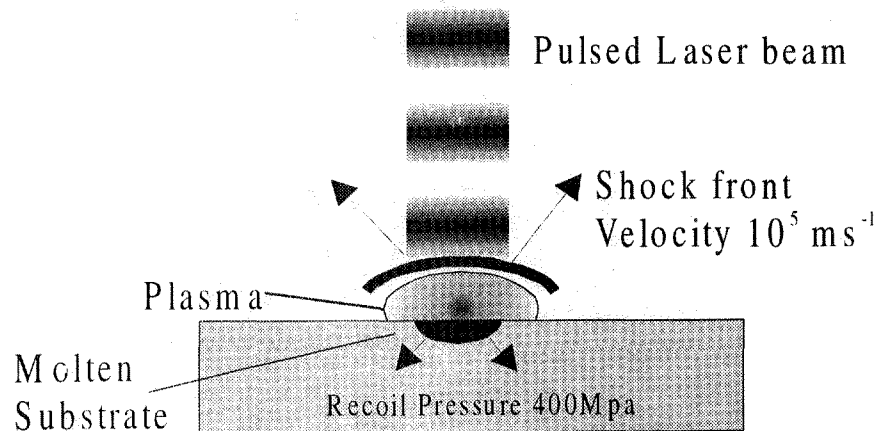


Figure.2 Interaction of a Q-switched laser pulse and the associated shock wave.

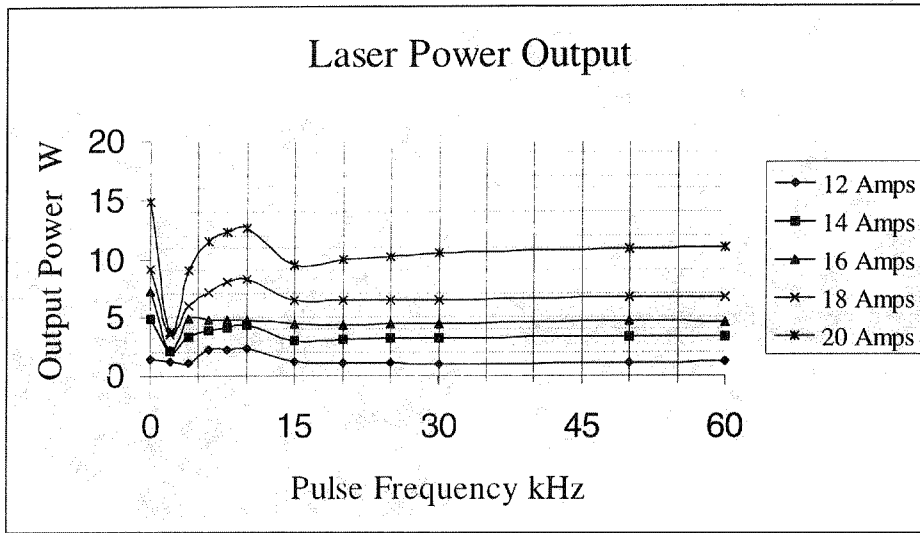


Figure.3 Laser power output characteristics

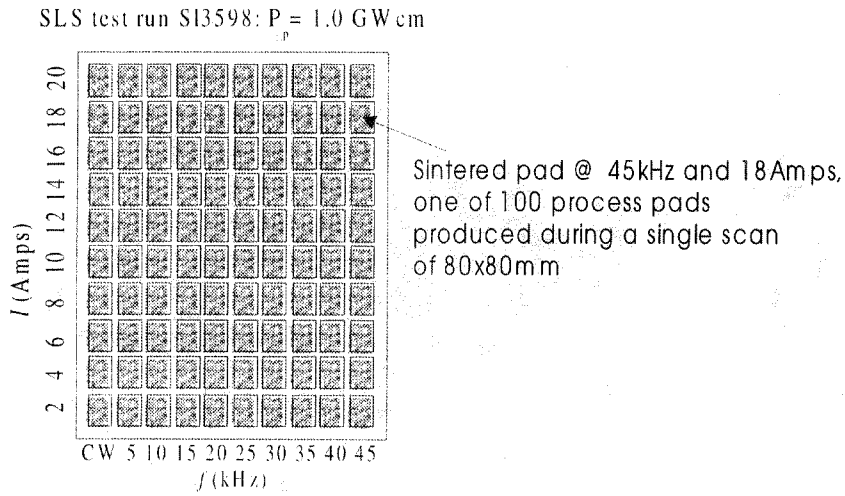


Figure.4 Schematic arrangement of interaction tests showing individual pads.

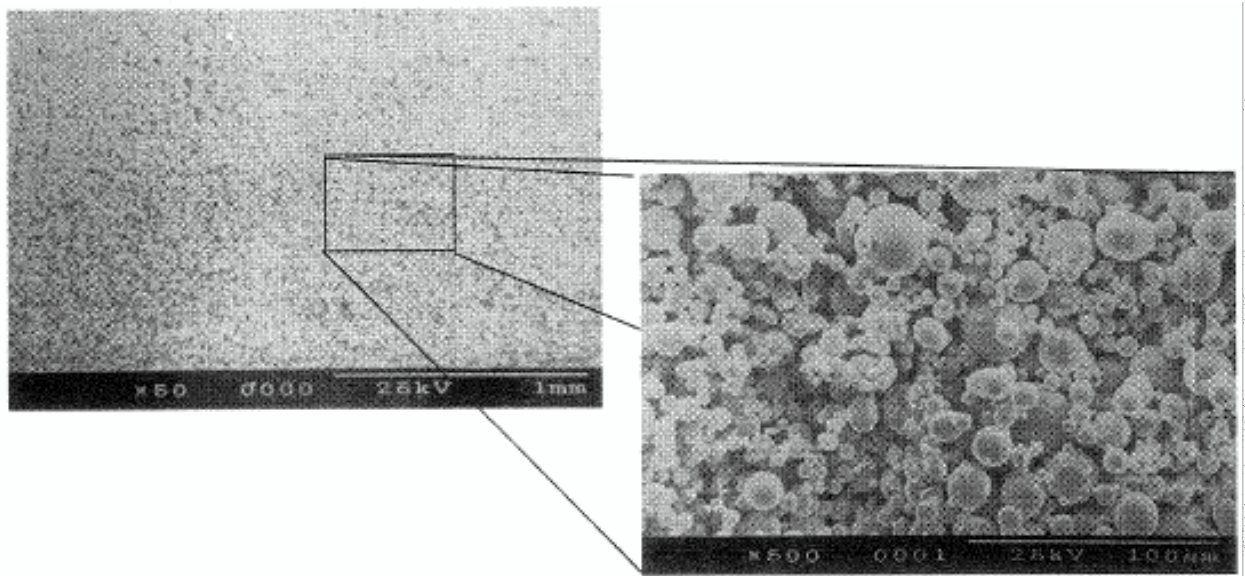


Figure.5 SEM of the unexposed powder bed at 50x magnification with inset at 500x magnification..

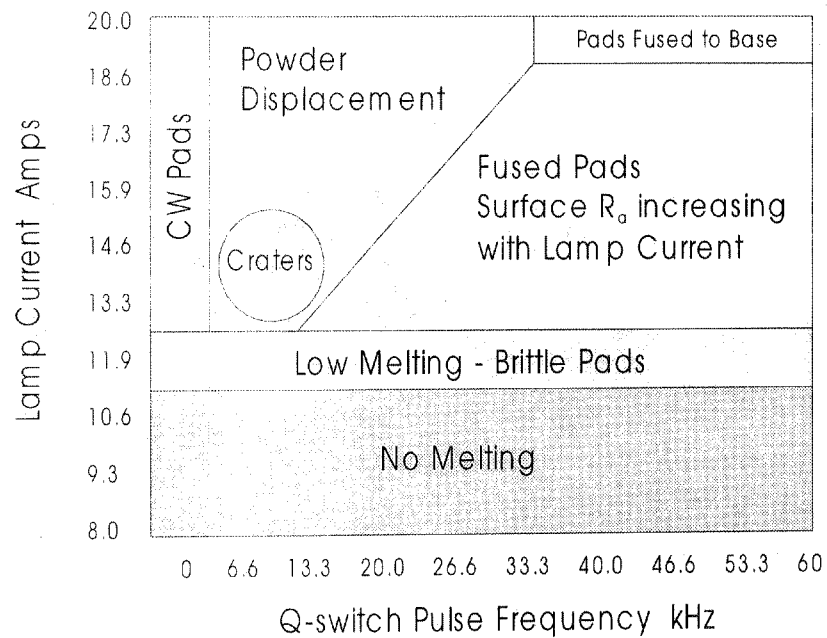


Figure.6 Process map of laser-powder interaction, laser beam diameter 50 μm.

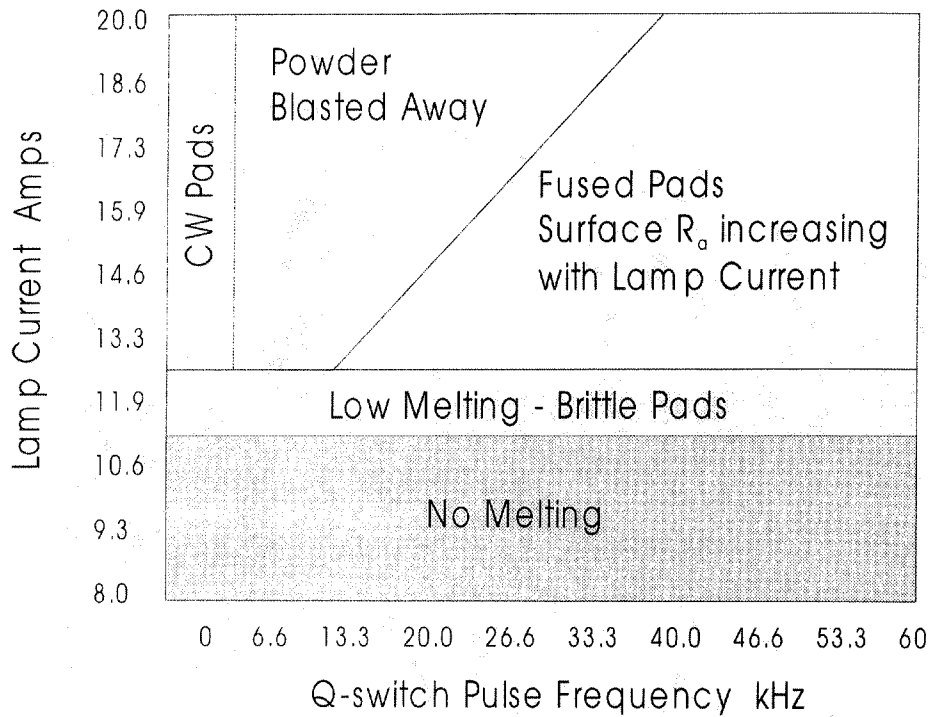


Figure.7 Process map of laser powder interaction, laser beam diameter 150µm.

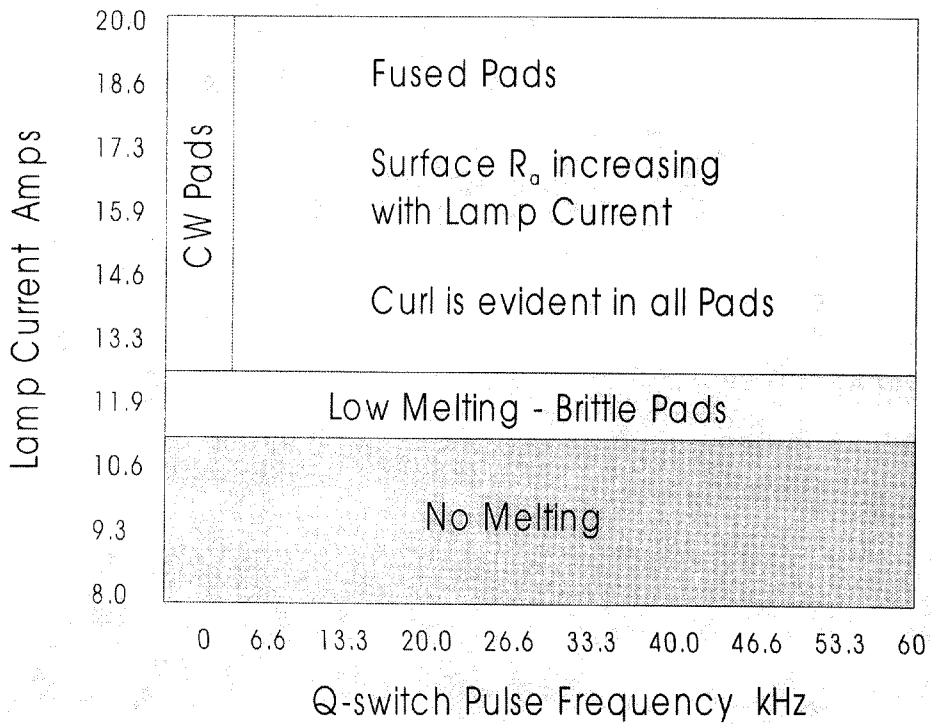
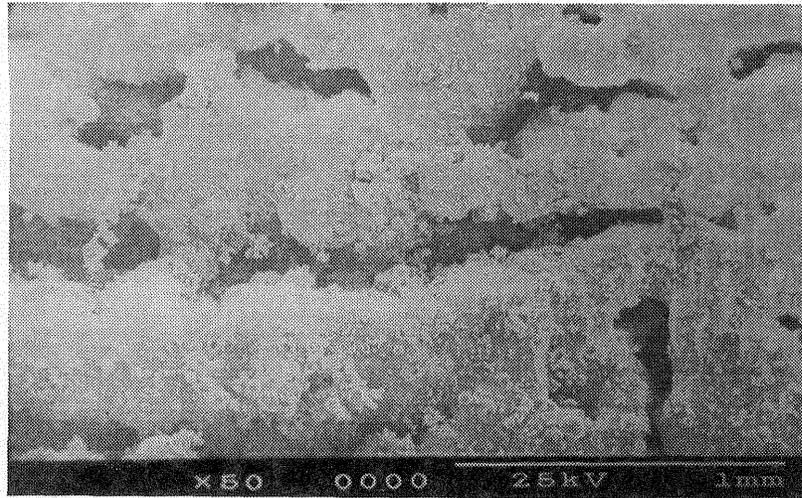
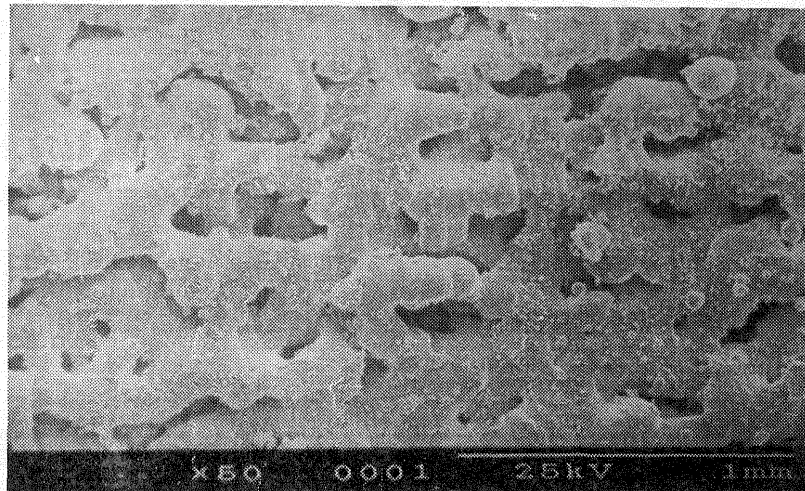


Figure.8 Process map of laser powder interaction, laser beam diameter 300µm

a)



b)



c)

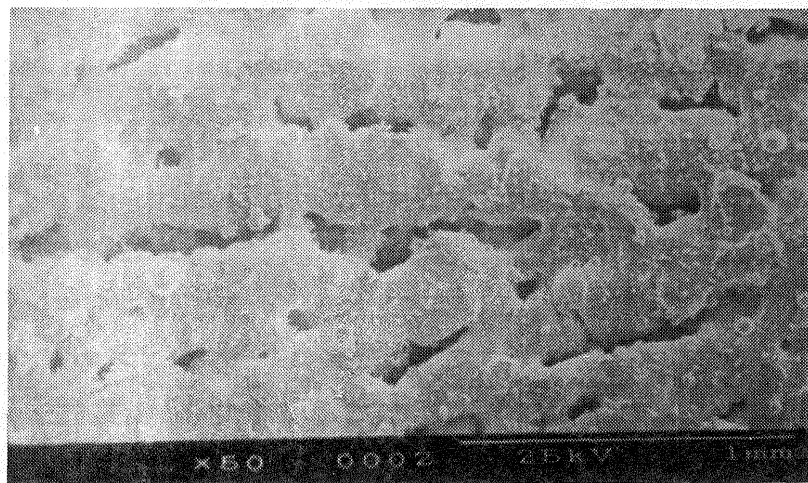


Figure.9

*micrographs of pads produced using a beam diameter of 150 μ m
a) CW @ 20A and 15W, b) 40kHz @ 20A and 11W, c) 60kHz @ 20A
and 12.6W.*

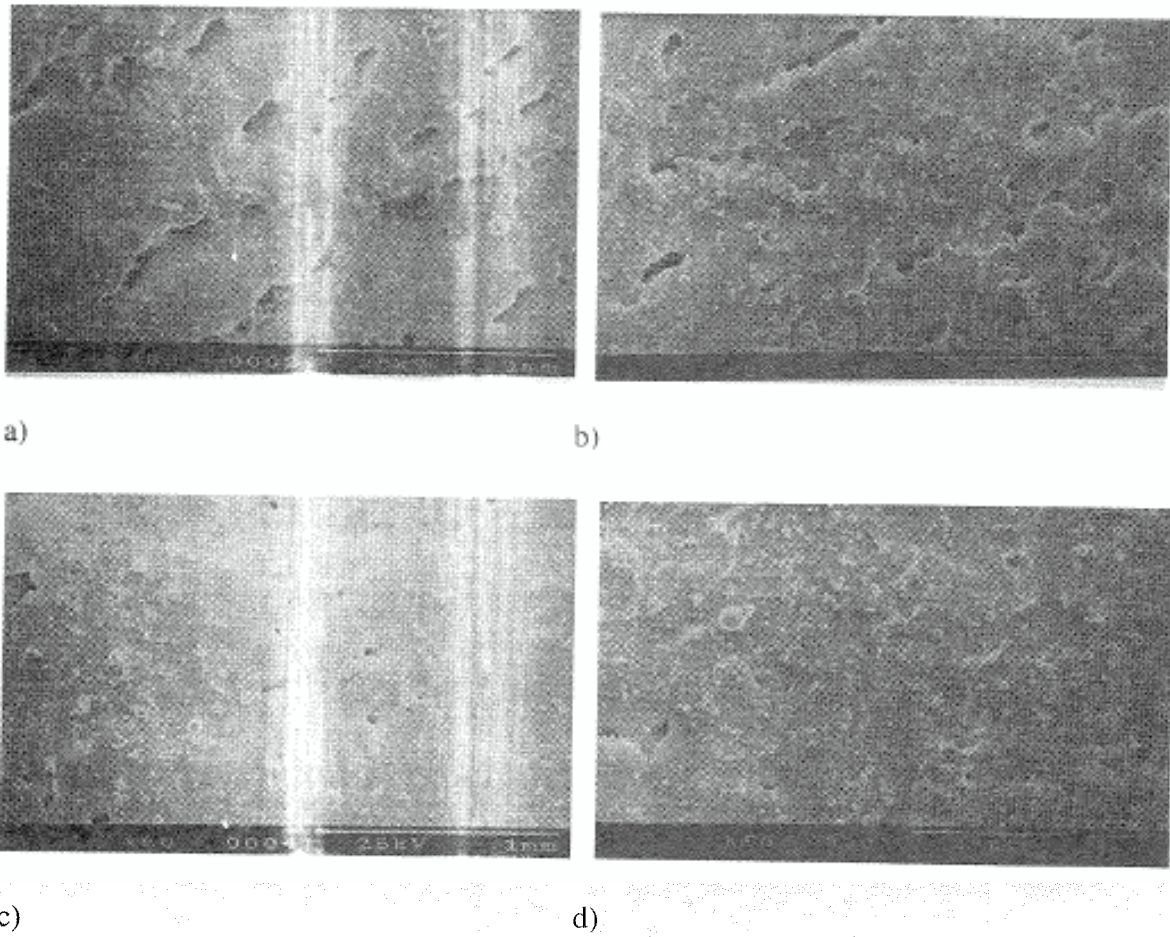


Figure.10 micrographs of pads produced using a beam diameter of $300\mu\text{m}$
 a) CW @ 20A and 15W, b) 20kHz @ 20A and 10W, c) 40kHz @ 20A
 and 11W, d) 60kHz @ 20A and 12.6W.

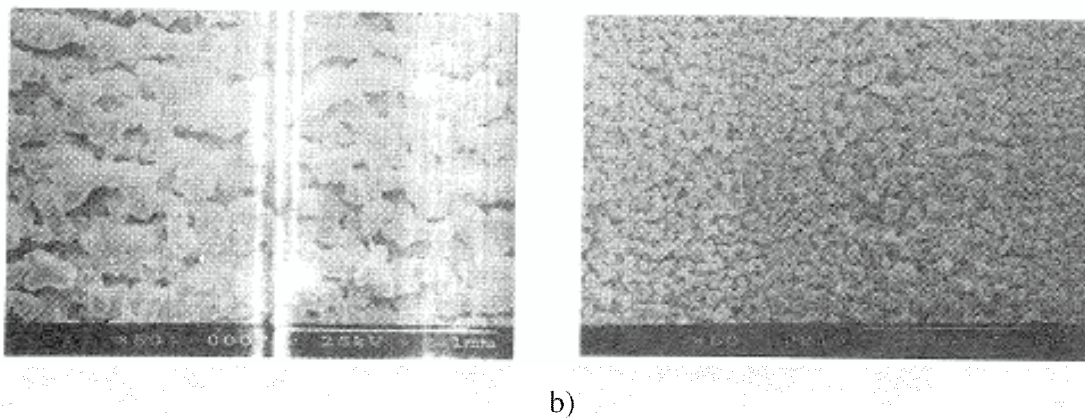


Figure.11 micrographs of pads produced using a beam diameter of $200\mu\text{m}$
 a) CW @ 13.3A and 4W, b) 60kHz @ 13.3 A and 4.4W.

